REVISTA MATÉRIA V.29 N.2
ISSN 1517-7076 article e20230368, 2024

Analysis of mechanical performance and durability of repair mortar with partial replacement of tufa stones with aggregates

Ramakrishnan Subramanian[1], Yogeshwaran Venkatraman[1]

[1]Sri Krishna College of Engineering and Technology, Department of Civil Engineering. Coimbatore, India.
e-mail: srkcivil@gmail.com, svyogi23190@gmail.com

ABSTRACT

In this study, the mortars utilized in the restoration projects need to be compatible with the conventional materials that were first used in these structures, both in terms of their mechanical and physiochemical qualities. Here, varying proportions of tufa stone powder – 37 and 42 percent by weight of the mixture, are used to partially replace the fine aggregate mixed mortars for repairs (M1, M2). In order to compare the performance of the third type of mortar (M3) with the tufa stone-based combinations, it was used in addition to the previously made mortars (M1, M2). The three types of mortars were thoroughly evaluated by examining their mechanical properties and durability qualities in conjunction with the tufa stone. The prepared mortar M2, out of all the mortars tested, which had a higher percentage of tufa stone powder substitution and a lower binder content, performed the worst mechanically, according to the data. The compressive and flexural strength of M2 mortar mix is 1.12 MPa and 0.72 MPa tested at 28 days. Similarly, the UPV, shear strength and shear interface for the M2 mortar mix is 0.71 MPa, 0.52 MPa and 1208 m/s at 60 days respectively. This implies that in comparison to the traditional tufa masonry, this specific mortar is less compact and more flexible. The created mortar (M2) has similar thermal qualities and is long-lasting like tufa stone found in historical sites.

Keywords: Mortar repair; Tufa stone; Robustness; Physical and Mechanical properties; Characterization process.

1. INTRODUCTION

Deterioration of building materials can take many forms throughout time, including mechanical, chemical, mineralogical, and physical changes. There are several reasons why components in old buildings deteriorate. This usually takes place at the interface where the material meets the environment or where it meets another substance. The inherent qualities of the construction material, which include its kind, attributes, mass distribution, origin, processing techniques, historical significance (previous preservation efforts), compatibility and blend-in with other materials, and more, control this procedure. Environment also has a role in determining when degeneration begins and how fast it advances. It is important to choose repair construction materials for restoration projects that are compatible with the original materials used in these historic buildings in terms of their mechanical qualities, chemical and mineralogical makeup, and visual similarity [1]. For this reason, ensuring total compatibility (physical, chemical, and structural) between the old stone and the repaired mortar is an essential prerequisite for conservation and restoration projects. To ensure that the repair mortar performs as best it can, compatibility is necessary. The Latin term “tofus” which meaning “a spongy stone,” is whence the name “tufa” originates, denoting the stone’s great permeability. Throughout history, historical structures in several parts of France have frequently used tufa, a common French limestone. It has very good physical properties and white in color and the stone is easily found in the Loire Valley and was heavily utilized in the building of historical buildings there, especially for their façade [2]. As such, this stone has already been the focus of a great deal of research. Tufa stones are usually shaped into consistent sizes in quarries using technology. These stones are then brought to the closest manufacturing facility. A substantial amount of colloidal waste is generated during the production process when sand and water are combined, which is harmful to the environment. As disposal costs rise, it becomes economically unfeasible to dispose of this trash [3]. Therefore, it became necessary to discover solutions for this problem by repurposing these waste products, even in small amounts. Reuse and recycling techniques have, in fact, been increasingly well-known in the building materials industry in recent years. Tufa powder can be used again as a partial an alternative to aggregate or cement in concrete and cement mortar due

Corresponding Author: Ramakrishnan Subramanian Received on 19/12/2023 Accepted on 29/02/2024

DOI: https://doi.org/10.1590/1517-7076-RMAT-2023-0368

to the similarity in their mineral makeup and physical attributes [4]. This alternative can be used for a number of purposes, such as historic building restoration mortar. The components of restorative mortars come in a wide variety and include many different compounds. Because lime has a long history of use in historical landmark and monument repair mortars in European countries, among these mortars, it is the most widely recognized binder. Prior research work analysis indicated that cement and lime were compatible when used in repair mortar compositions [5]. When used with ancient stone, this has a positive effect on the restoration mortar's efficacy since the physical, chemical, and mechanical qualities line in a highly desirable way. As a result, the repair mortar mixture's proportions need to be thoroughly thought out, and choosing extra ingredients and their qualities call for a high level of accuracy [6]. For this reason, precise experimental research should be used to determine them. When the prepared mortar is first applied, it should be done so with the intention of maintaining and improving the historical building's exterior appearance from an architectural and historical standpoint. It is imperative that the original and processed mortars' micro structural properties show similarities in their use as building materials [7]. The constructed mortar should not be substantially weaker or stronger than the original stone from a mechanical standpoint. A balanced strength in relation to the original materials must be attained. Variations in the components' strength and stiffness might weaken the binding between the ancient stone and the prepared mortar, impacting the connection over time as well as in the immediate term. On the other hand, it is expected that the prepared mortar will boost the old stone's resilience against adverse environmental factors and extreme exposures [8]. The purpose of this research was to produce repair mortars with the efficient utilization of leftover tufa stone powder by partially substituting it for fine aggregate. The objective was to create a repair mortar that works well with tufa stone when restoring historic sites. To assess the suggested repair mortar's suitability through experimentation, a different composition is created. The experimental analyses include assessing the mechanical characteristics of each recommended repair mortar formulation in an effort to choose the best restoration mortar that blends in with the stone and the old mortar. The temperature and durability characteristics of the recommended repair mortars were also assessed, as they were important considerations in determining whether or not tufa stone powder should be used as a portion of the combined repair mortar mix component.

2. MATERIALS AND METHODS

2.1. Materials

White cement with different grades of 33, 43 and 53 are available in India and this experimental study 33 grade of cement was used. The properties of 33 grade white cement are discussed in Table 1. Around 93% of the air lime's composition was calcium hydroxide, in accordance with hydrated lime (EN 459-1) [9]. Tufa stone powder is a waste particle that is produced as a result of cutting tufa stone. Usually, the size of its particles varies between 0.5 and 80 μm. Table 1 lists the physical and mineralogical characteristics of the tufa stone powder and air lime. The fine aggregate employed in this study is silica sand, which has a bulk density of around 1.22 g/cm^3 with particles ranging in size from 20 to 315 μm. Figure 1 shows the distribution of particle sizes for the silica sand and tufa stone powder. Every mortar that is manufactured uses regular tap water. The bonding and adhesion between old tufa stone and the mortar was improved by adding Sika Visco-bond admixtures. The old tufa stone was procured from France and used for these experimental investigations. This stone's main characteristics are its white hue, its comparatively a 1.31 g/cm^3 light bulk dry density, and its reputation for being sculpturally simple when used in historic building repair and rehabilitation. According to mineralogy, calcite and silica make up

Table 1: Physical, chemical and mineralogical characteristics of used materials.

TYPE OF CHARACTERISTICS	UNITS	33 GRADE – WHITE CEMENT*	AIR LIME*	POWDERED TUFA STONE*	ROCK TYPE – TUFA STONE*
Bulk density (dry)	g cm^{-3}	–	0.41	0.89	1.29
Blaine surface	cm^2 g^{-1}	4900	10580	–	–
Porosity	%	–	–	–	50
Skeletal density	g cm^{-3}	3.09	2.14	2.49	2.49
Compression strength	MPa	51	–	–	–
Composition of minerals	Wt%	C_3S = 72 C_2S = 11 C_3A = 10	$Ca(OH)_2$ = 90 Calcite = 4.2	Calcite = 47 CT opal = 25 Mica & Clay = 9 Quartz = 9	Calcite = 47 CT opal = 25 Mica & Clay = 9 Quartz = 9

*Data received from the manufacturer.

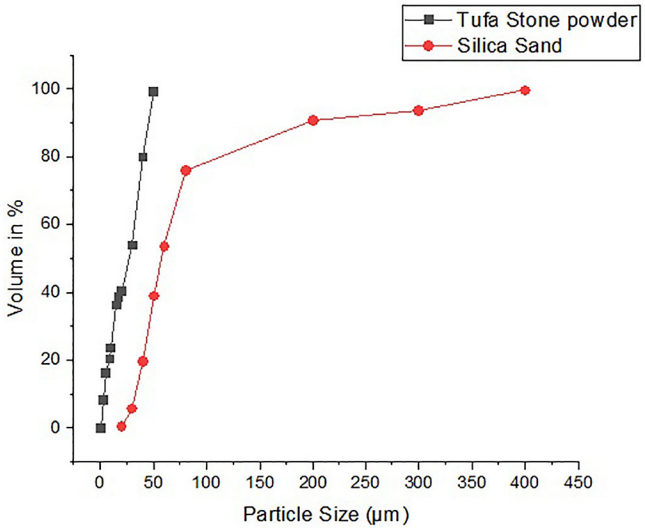

Figure 1: Tufa stone and silica sand – particle size distribution.

Table 2: Mortar mix proportions for experimental study.

MORTAR TYPE	% OF BINDER	TUFA STONE POWDER (wt %)	SILICA SAND (wt%)
M1	White cement 1/3 Lime 2/3 (25%)	37	38
M2	White cement 1/3 Lime 2/3 (15%)	42	43

the majority of tufa stone, as seen in Table 1. Apart from that, the stone has a porosity of about 48% and a wide variety of pore diameters, from 0.003 to 20 µm. Because of these properties, the stone's 10 MPa compressive strength is rather low.

2.2. Mortar preparation

Two different types of mortars (M1 and M2) were used for this experimental study. The tufa stone powder along with air lime, white cement and silica sand was used in different ratios as indicated in Table 2 for each mortar creation. Different amounts of binders were present in the two produced mortars (25% and 15%). Comprising two thirds lime and one third white cement, the ratio of each binder stayed the same for every mortar that was made. At two different percentages (37% and 42%) according to the total weight percentage of the mixture, tufa stone powder was employed to partially replace silica sand. As a result, each prepared mortar had a different amount of these two ingredients, as shown in Table 2. Both prepared mortars had a water-to-cement ratio of 0.4. The prepared mortar specimens were stored in the constant temperature of 25°C. The mortar (M1 & M2) has skeleton and bulk densities of 1.89 and 1.21 g/cm^3 respectively. A restoration mortar with the designation M3 (LEGASTON R), available from Véga Industries, was selected for the study in addition to the two pre-made mortars. Due to the fact that this mortar is composed of limestone sand, lime, and certain ingredients, it can be used to replace or repair delicate stones that have chipped or fractured [10]. This proprietary production mortar's precise mix proportions were kept a secret because it is a novel product. Its bulk density was found to be 1.62 g/cm^3, whereas its skeleton density was 2.17 g/cm^3.

2.3. Experimental methods

2.3.1. Pore distribution and porosity

One of the most important physical properties of any porous material is its total porosity (ØT). The overall porosity of tufa stone and mortar specimens were calculated using twenty samples (Table 3). For each set of

Table 3: Details of tested specimens in experimental study.

TYPE OF THE PROPERTY	TYPE OF THE SPECIMEN	DIMENSIONS OF THE SPECIMEN (cm)
Porosity	Irregular shape and small pieces	4.5 to 9.5 cm^3
Compression strength	Cylinder	4 × 4
Flexural strength	Prism	4 × 4 × 16
UPVC	Cylinder	4 × 8
Shear strength	Cylinder	4 × 4
Capillary water absorption	Cylinder	5 × 5
Thermal conductivity	Cylinder	0.5 × 2
Permeability of Gas	Cylinder	5 × 5
Permeability of water	Cylinder	4 × 4

five specimens, the average total porosity was determined. A mercury intrusion porosimetry (MIP) test was performed to ascertain the distribution of pore diameters. A Micropore IV 9520 Auto pore micro-porosimeter that could produce pressures between 2.76 kPa and 414 MPa was the equipment used to measure pore sizes between 0.003 and 450 μm. Three specimens of stone and mortar were examined, and the mean value was obtained for each set of tests.

2.3.2. Compression and flexural strength

The compression and Flexural testing were conducted for all the specimens using the testing machine (Instron 4485) with 250 kN capacity and rate of loading is 0.2 mm/min. A flexural bending test with three points was used. Twelve specimens underwent tests at 14, 28, and 60-day intervals (refer to Table 3). Three-point loading procedure (EN 1015-11) [11] was conducted for the experimental procedures. Based on sets of three readings for each measurement, the average flexural strength value was noted. Adherence to the standard NF-P94-420 [12] requirements was ensured during the evaluation of compressive strength. The mortar and tufa stones were tested in 14, 28 and 60 days using twenty cylindrical specimens of four centimeters in diameter and height. For each measurement, sets of five specimens were used to calculate the reported average compressive strength value.

2.3.3. Shear strength

As shown in Table 3, tests were conducted on saturated cylindrical specimens at 14, 28, and 60-day intervals. Each specimen, as shown in Figure 2, was made up of two centimeters of sticky mortar and two centimeters of constructed tufa stone. In compliance with ASTM D3080-11 [14], the direct shear strength test a method commonly employed in geotechnical evaluations was employed to ascertain shear strength. The specimen was placed in the area between the two proportionately moving bisected pieces of the box. The top of the section was kept in fixed state and the bottom section is moved at the loading frequency of 0.5 mm/min in this experimental process. A loading circle connected these parts, making it easier to quantify shear loads, as seen in Figure 3. The resultant lateral forces efficiently illustrate the friction state at the mortar-stone interface by representing the stress applied to the specimen's shear plane. Twenty specimens were tested, and for each measurement, sets of five specimens were used to calculate the mean shear strength value.

2.3.4. Thermal conductivity

The conventional hot wire method was used to measure thermal conductivity, adhering to the ASTM D5930-97 [15] standard's instructions. Twenty samples were baked at 60°C for 48 hours. The pulse velocity of ultrasonic was recorded for each specimen in accordance with the guidelines provided in the NF-P94-411 [16] standard. 82 kHz tiny wave frequencies Pundit equipment was used to measure the wave passage velocity. Specimens were evaluated for ultrasonic pulse velocity at 14, 28, and 60-day intervals. The average of five measurements was represented by each ultrasonic pulse velocity value that was recorded. After that, they were evaluated after 28 days after being encased in plastic films (as shown in Table 3). Thermal conductivity was quickly determined using the FP2C device. That required connecting two specimens with the same geometry directly using a hot wire. Since the evolution of temperature is correlated with the logarithm of time, the thermal conductivity is calculated. Using the chosen nickel-type hot wire, an electrical current is created through the specimens to raise their temperature. All during the test, the specimens serve as an unlimited medium. For each five-piece set, we recorded the average heat conductivity coefficient value. For a total of twenty specimens, thermal expansion was

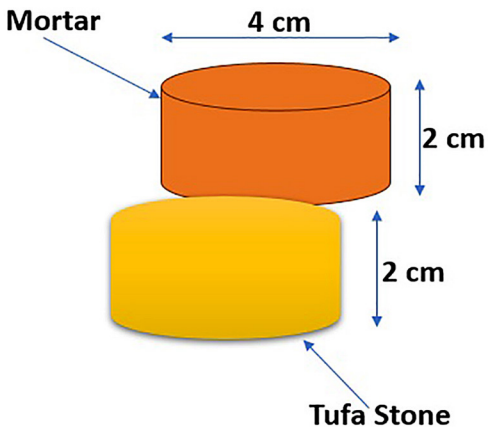

Figure 2: Shear test specimens – mortar and tufa stone [13].

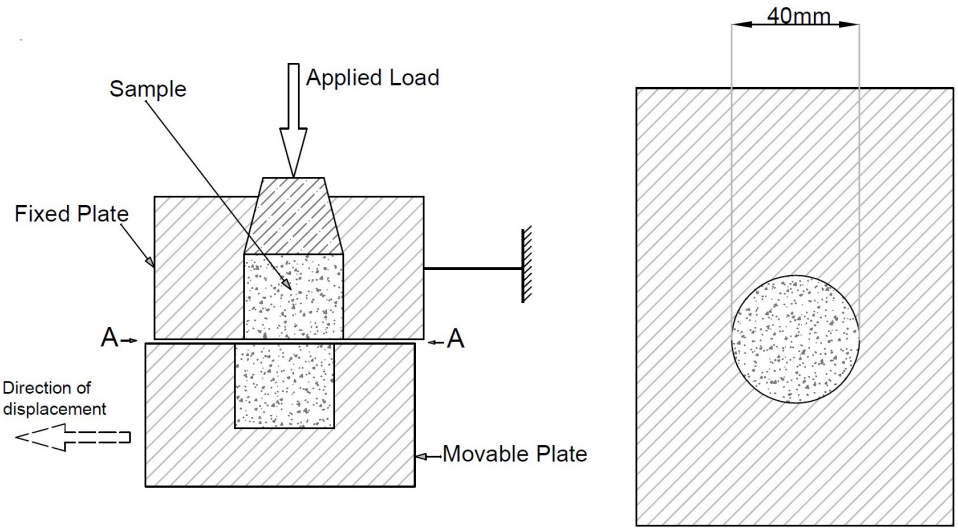

Figure 3: Shear strength testing setup [13].

evaluated using a LINSEIS TMA PT1000 device. When a specimen is exposed to varying temperatures, such as 20, 40, and 60°C, thermal expansion can be evaluated. Before any defects were measured, each specimen was given a full day to stabilize. To keep the samples from drying out, they were covered in plastic before being analyzed after 28 days. For every measurement, sets of five specimens were used to obtain the average coefficient of thermal expansion.

2.3.5. Ultrasonic pulse velocity

For twenty specimens in all, ultrasonic pulse velocity measurements were performed in accordance with standard NF-P94-411 (see Table 3). A device called Pundit was used to test the wave passage velocity at a tiny wave frequency of 82 kHz. For every specimen, ultrasonic pulse velocity measurements were made at 14, 28, and 60 days. The recorded values are the average of five observations each.

2.3.6. Capillary water absorption

The Washburn model is used to estimate the height of water in a vertical cylindrical porous pipe without taking gravity into account. Two distinct imbibition factors can be obtained using this technique (A and B). Both the anterior capillary height and the mass uptake curve (M) inclination with regard to the time spent squared were in line with these two factors. Actually, the capillary water absorption test demonstrates how the characteristics of the porous medium influence imbibition activity and provides a better explanation for the kinetics of imbibition

over time (h and M). Finally, using the following equation, the capillary porosity (Nc) can be determined from this test: $A = \rho_{water}.BNc$. Twelve dried specimens from earlier were tested in accordance with EN-1925 [17]. Three measurements from mortar and stone samples were used to calculate the average capillary absorption coefficient.

2.3.7. Permeability of gas and water

The water permeability test was shown to be an efficient method of obtaining further information on the water transfer characteristics of the specimens under investigation. This test was performed on twenty specimens (Table 3). In order to guarantee that the specimens were fully saturated, the vacuum saturation procedure was utilized. Water permeability was measured using a high-pressure triaxial cell in the range of 10–16 m/s. A hydraulic pressure system that was automated was used to maintain a constant head pressure. To make sure the Darcy law could be used correctly, the condition of stability was confirmed prior to the test. In order to guarantee that the specimens were properly saturated, a bottom-up water flow direction was used during the test to keep air bubbles from becoming trapped. Additionally, an automated hydraulic system was used to apply confining pressure to the specimens. By keeping the confining pressure marginally greater than the applied head pressure, the system produced a unidirectional flow of water. Each measurement was broken down into sets of five readings to determine the average coefficient of water permeability. Statically compacting mortar inside a stainless-steel cylinder mold generated twenty samples for the test of gas permeability, as shown in Table 3. The test protocols were followed when measuring gas permeability at the designated curing age. Each property was measured in sets of five, from which the average coefficient of gas permeability was determined. The specimen kinds and dimensions are shown in Table 3 along with these characteristics.

2.3.8. Microstructural analysis of mortar

Under various operating circumstances, the surface behavior of the mortar mixes (M1 and M2) was examined using Fourier Transform Infrared Radiation (FT-IR) and Scanning Electron Microscopy (SEM) with X-ray Diffraction (XRD). These investigations were carried out to find out how well tufa stone powder performed with silica sand and how it interacted with cement particles to increase the mechanical strength of mortar mixtures. Based on the findings from the mechanical strength of each mortar mix, the microstructural analysis was looked at in this study to find the best blends.

3. RESULTS AND DISCUSSION

3.1. Porosity and pore size distribution

The pore size distribution curves for all mortar samples and the tufa stone, as determined by the Mercury Intrusion Porosimetry (MIP) test, are shown in Figure 4. All of the measured porosities are displayed in Table 4, and Figure 4 shows the MIP test results. The produced mortar M3 seems to work best with pore widths of 0.6 μm and 1.6 μm, as shown in Figure 4. The fact that peaks are present at these two diameters suggests that this mortar has the best porous structure for the material. For the constructed mortar M1, pore diameter shows two separate peaks at 2.5 μm and 1.6 μm in Figure 4. This shows that the pore structure of mortar M1 is somewhat coarser than that of manufactured mortar M3. However, the mean pore diameter of the mortar (M2) is 2.5 μm. When compared to tufa stone, which shows a clear peak at 8.4 μm, all three mortars' claimed pore diameters are much lower. These results certainly match the overall porosity values shown in Table 4. It appears that the mortar's porous composition is significantly influenced by the binder content. For instance, mortar M1, which has a 25% binder concentration, is less porous than mortar M2, which is made with a 15% binder percentage. In fact, the mortar's microstructure is greatly influenced by the amount of aggregate utilized. For mortar M2, adding a 42% replacement of the total aggregate resulted in higher porosity, which reached 47% overall. This implies that an increase in the aggregate substitution rate leads to an increase in the total porosity. It seems that adding more lime to the mortar paste also known as the binder reduces part of its porosity and improves its homogeneity [18]. Additionally, as the lime rate increases, the distribution of pore sizes shifts, increasing the number of smaller pores. Because the binder concentration varied and tufa stone powder was partially substituted, the resulting mortars, M1 and M2, displayed varying degrees of hydration and carbonation reactions. The aggregate particles operate as nucleation sites for the creation of freshly configured calcite crystals due to their structural similarity to the binder and the limestone particles' ability to stimulate carbonation processes. Indeed, during the early phases of hydration, limestone offers a surface that is ideal for C-S-H gel formation and growth. This considerably quickens the process of hydration [19]. The calcite crystals tend to bond with the surrounding aggregate particles and resemble tiny versions of portlandite crystals. This interaction helps to limit the total porosity and increase the mechanical strength of the material by promoting the creation of smaller

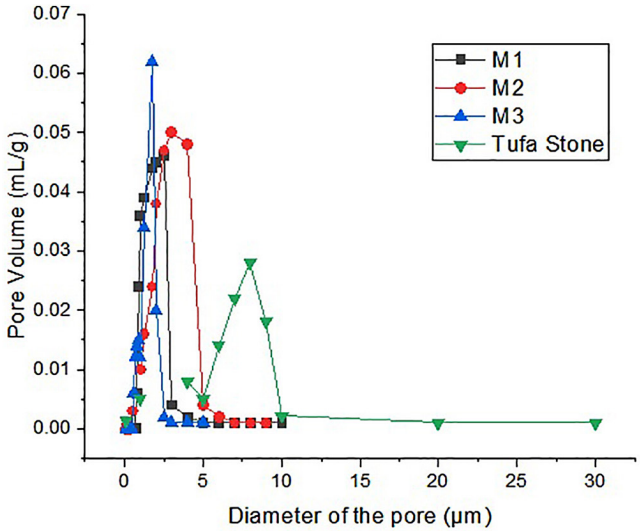

Figure 4: Pore distribution of tufa stone and mortars.

Table 4: Tufa stone and mortar – porosity values.

TYPE OF MATERIAL	TOTAL POROSITY IN %
Mortar (M1)	41.94
Mortar (M2)	46.15
Mortar (M3)	28.42
Tufa stone	47.68

pores. Specifically, because there are fewer nucleation centers and less packing density in the mortar M2 binder as a result of the lower lime content, the carbonation process is less effective [20]. These elements are necessary to sustain carbonation and hydration reactions as well as the crystallization of calcite [21]. As a result, there was a reduction in density and an elevation in porosity within the pore structure, featuring an average pore diameter of 2.5 µm and an overall porosity of 47%. Since there are fewer nucleation centers and less packing density to facilitate hydration, carbonation reactions, and the creation of crystalline calcite, the lower lime content in the mortar M2's binder results in an unsuccessful carbonation reaction [22]. Thus, as can be seen from Table 4 and Figure 4, which display a total porosity of 47% and a mean pore diameter of 2.5 µm, respectively, the pore structure becomes less compacted and more porous. Understanding the properties of the pore structure in the mortar is crucial to ensure compatibility with old masonry. Hence, mortar M2, with porosity levels similar to tufa stone and a less compacted pore structure, is less compatible with the stone. When crystallization pressure was applied to the mortar, which had a lesser percentage of fine pores, the stone could deteriorate [23].

3.2. Mechanical properties

3.2.1. Flexural and compressive and strengths

The flexural strength and compression strength of tufa stone and mortar mixes (M1, M2 & M3) are shown in Figure 5 and Figure 6 respectively. The results shows that the tufa stone has higher strength compared to other three types of mortars. At all ages (14, 28, and 60 days), M2's flexural and compressive strengths were consistently lower than those of the other mortars (M1, M3). The very limited properties of M2, namely its strength, toughness, and deformability, may be useful for restoring and maintaining historic sites. In these landmarks, M2 may act as a protective covering for the ancient tufa stone. No matter where the degradation comes from, this protective layer would take it all in, making sure that any deterioration happens inside this layer (the prepared mortar, M2) and does not affect the original stone itself, keeping it intact. As mentioned earlier, the hydraulic elements hydrate at a slower pace as a result of the decreased binder quantity shown in mortar M2. This is because the mortar's silica components and air lime have limited pozzolanic reactions, which cause the reaction process

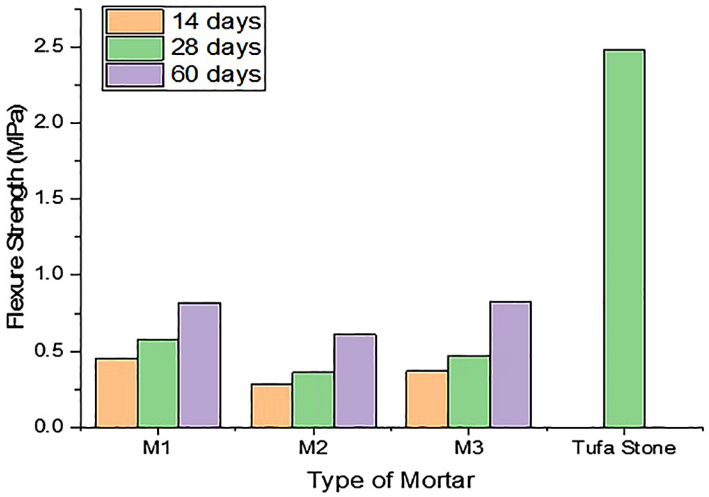

Figure 5: Tufa stone and mortar – flexural strength at the ages of 14, 28 and 60 days.

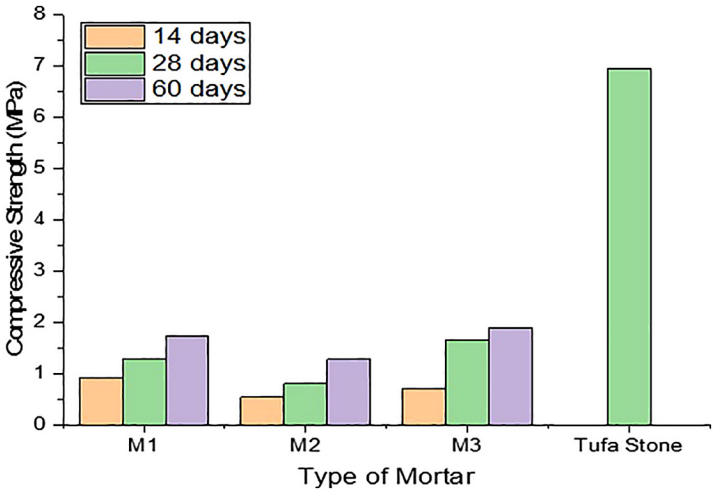

Figure 6: Tufa stone and mortar – compression strength at the ages of 14, 28 and 60 days.

to produce more portlandite [24]. As a result, this restriction limits the quantity of hydrated products that can be generated in pozzolanic reactions. In a similar vein, the mortar's lower lime content decreased the silica components' solubility and reactivity, which in turn caused the pH to drop. AKYÜNCÜ and AVŞAR [25] indicates that an ineffective carbonation reaction occurs because to the lower lime content in the M2 binder. The trace amount of calcite in the limestone powder is insufficient to act as a nucleating agent to promote crystal growth when portlandite is carbonated [26]. As shown in Table 4 and Figure 4, this results in a higher total porosity and the development of a less dense pore network inside the mortar's structure. As a result, this weakens the mortar. The created mortar M1, on the other hand, had superior packing density. It contained 25% binder and substituted 37% of the tufa limestone powder. As a result, there were more nucleation agents available to assist the carbonation and hydration events, which promoted the development of rock crystal [27]. The decrease in open porosity led to strengthening, and as Table 4 and Figure 4 illustrate, the distribution of pore diameter started to exhibit two peaks at 2.5 and 1.6 µm. In contrast to tufa stone, M2 has reduced compressive and flexural strength. In reality, this feature is helpful for the envisioned use of the refurbishment mortar, especially for the connection of old mortars and brickwork components [28–31].

3.2.2. Interface of shear

Figure 7 and Figure 8 depict the shear strengths at the mortar-stone contact and the final shear strengths of the mortars and tufa stone after 14, 28, and 60 days, respectively. The shear strengths of the mortars (M1, M2 and M3)

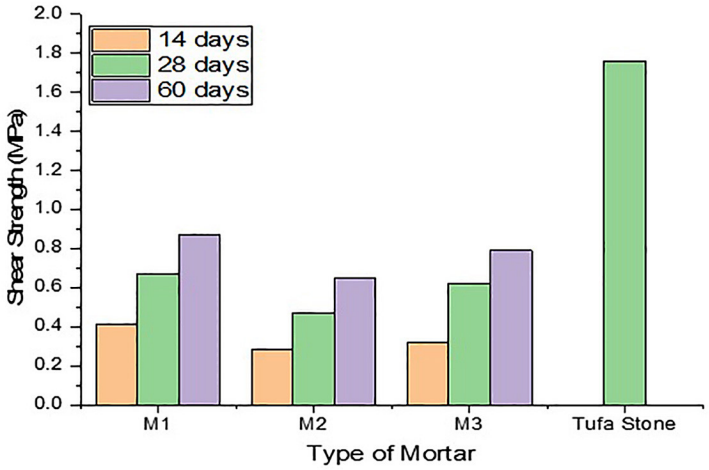

Figure 7: Tufa stone and mortar – shear strength at the ages of 14, 28 and 60 days.

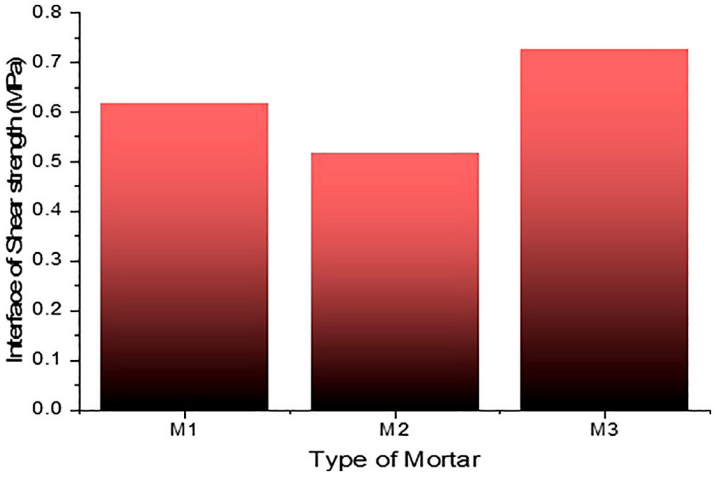

Figure 8: Interface of shear for different mortars.

mixes, as shown in Figure 7, although they are in no way comparable to the shear strength of the tufa stone. Figure 8 clearly shows that every mortar-tufa stone interface has shear strength data that show complete adhesion. The point where the mortar and tufa stone meet generally exhibits a high degree of adhesion [10]. This flawless adhesiveness appears to be displayed by the mortar at the interface with the maximum shear strength (M3). The chemical and mineral properties affect the mortar's ability to connect with the stone. Stated differently, it is contingent upon the characteristics of the stone-mortar contact surface, also known as the transition zone. In a similar vein, this component affected the strength under shear stress. A weaker component, whether it be in the mortar, the masonry, or at their interface, is the source of both cracks and failures [32]. This resulted in the rupture of the weakest part, repair mortar M2, since its confined shear strength was less than its strength at the stone interface. By doing this, you can be confident that it is appropriate and that any possible mortar failure won't impact the integrity of the tufa stone as long as it stays contained within and doesn't spread to the interface.

3.2.3. UPV analysis

Figure 9 shows the ultrasonic pulse velocity data for the tufa stone and the mortars (M1, M2, M3) that were used. The mechanical characteristics of a mortar, including strength, deformation behavior, and ultrasonic pulse velocity, can be greatly influenced the distribution of pore sizes and overall porosity within the mineral structure. Porosity exerts a substantial influence on the ultrasonic pulse velocity. A lower wave transition rate indicates more porosity in the mortar, which is associated with a weaker bond [33]. Consequently, as shown in Figure 9, the more porous mortar M2 displays the delayed and attenuated waves.

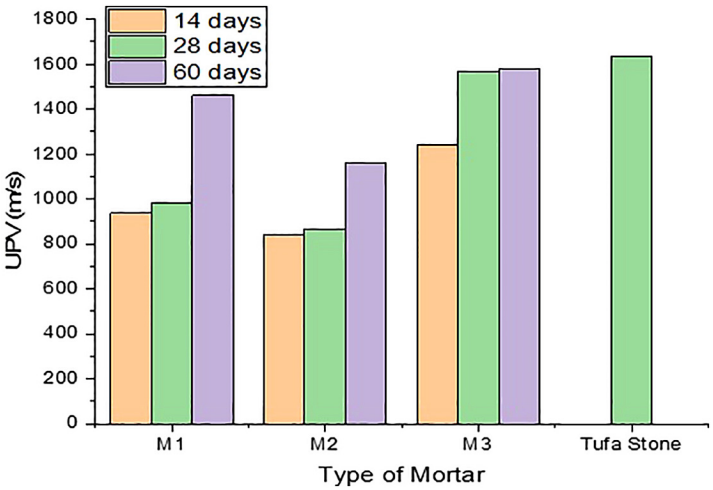

Figure 9: Tufa stone and mortar – Ultrasonic Pulse Velocity (UPV) at the ages of 14, 28 and 60 days.

3.4. Durability property of mortar and tufa stone

3.4.1. Thermal conductivity

Results of the dilatation and heat conductivity coefficients for the tufa stone and mortars are presented in Figure 10. The thermal dilation coefficients between M2 and the tufa stone were comparable, although different from those of M1 and M3. Furthermore, mortars M1 and M2's heat conductivity coefficients were similar to the tufa stone. When it comes to the preservation of old structures and historical sites, mortar M2 is a suitable material to use because of the comparable thermal properties it exhibits with tufa stone. The type and quantity of aggregate used, together with the amount of binder, can all have an impact on a mortar's thermal conductivity [34]. In terms of mortar M2, the configuration of its pore network and porosity has an effect on both dilation and heat conductivity. Because the mortar is porous, heat transfer is decreased and its thermal dilation is changed [35]. Larger pore widths may also result in higher heat conduction because they allow thermal bridges to form. Figure 10 illustrates that M2 had a greater thermal dilation coefficient than the repair mortar M1. Repair mortar M2's compatibility with tufa stone was confirmed by the fact that this coefficient value was almost identical to the tufa stone's dilation coefficient. The internal strains brought on by atmospheric changes can be effectively reduced by the convergence of the thermal dilation coefficients between the two elements, the tufa stone and the repair mortar M2 [36]. Furthermore, the similarity in thermal dilation supports the stable behavior of the tufa stone and mortar over a long time, especially when exposed to changes in the atmosphere.

3.4.2. Capillary absorption

With tufa stone and repair mortars, the capillary absorption coefficient is used to quantify the volume of water that is transferred through imbibition due to capillary action. Figure 11 illustrates the relationship between the square root function of time and the capillary front height for a range of mortars and tufa stone. The relationship between weight increase and capillary water, or water absorbed by imbibition, is shown in Figure 12 for both mortars and tufa at different curing times. Table 5 also displays the evolution of the imbibition coefficient for the stone and mortars, together with the mass coefficient (A) and visual coefficient (B). The water absorption heights of the tufa stone and the prepared mortar M2 are similar. On the other hand, when compared to the tufa stone, Figure 11 demonstrates that the manufactured mortar M3 and prepared mortar M1 have distinct water absorption heights. As shown successively in Figure 12 and Table 5, the weight increase resulting from absorbed water, as well as the mass and visual coefficients, demonstrated a convergence between M2 and the tufa stone. The findings specify that differences in water drive through capillary action were primarily influenced by the mix proportion of the repair mortar, particularly the quantity of binder and the amount of tufa stone powder replacement [37]. The water flow is constrained in repair mortar M2 in comparison to what could have passed through the pores of the tufa stone. The higher internal porosity and enhanced water absorption can be attributed to the calcic properties of the limestone particles [38]. Additionally, the presence of clay minerals in the limestone may have an impact on the moisture content of the repair mortar. When compatibility was considered, the water absorption by capillary action of the restoration mortar M2 was comparable to that of tufa stone. Due to

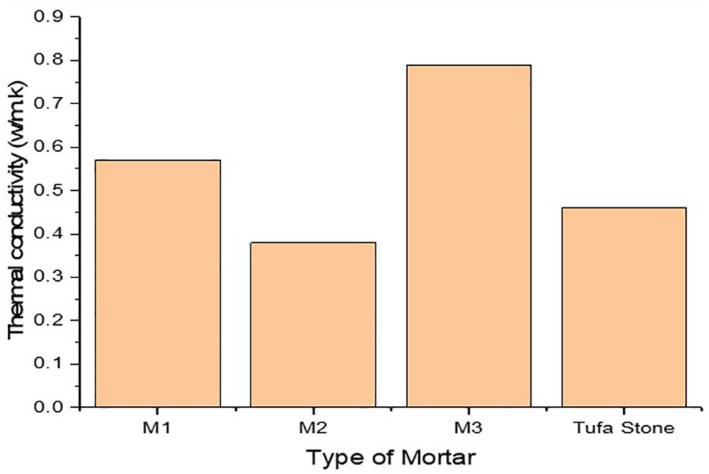

Figure 10: Tufa stone and mortar – thermal conductivity.

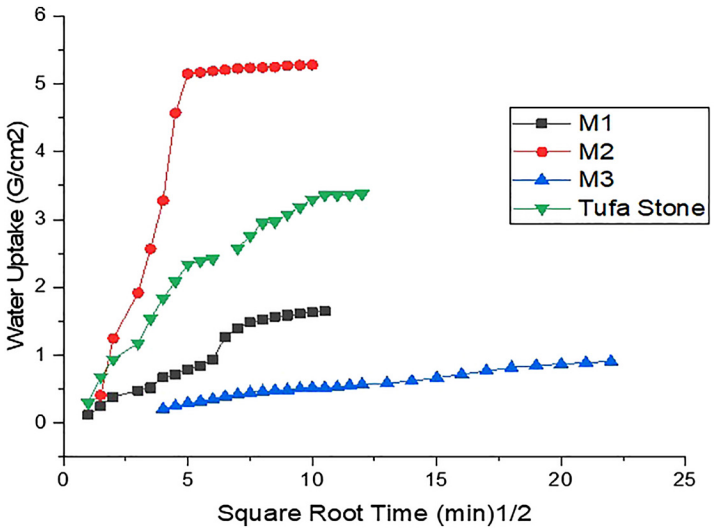

Figure 11: Tufa stone and mortar – imbibition results.

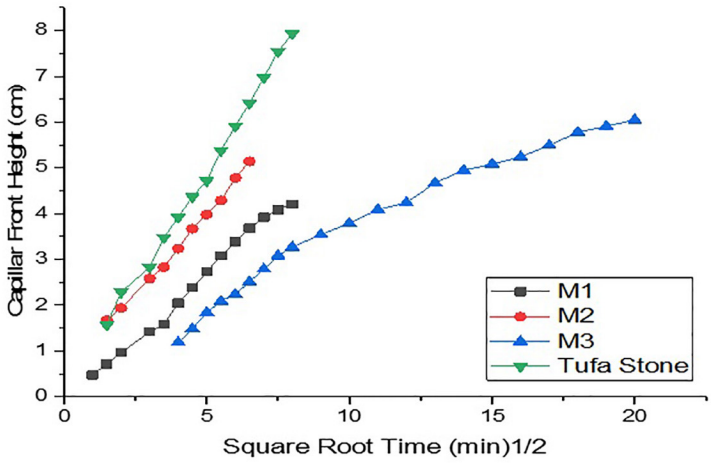

Figure 12: Tufa stone and mortar – water absorption results.

Table 5: Capillary water absorption of mortars and tufa stones – Experimental results.

TYPE OF MORTAR	CO-EFFICIENT OF MASS ($g/cm^2/min^{1/2}$)	CO-EFFICIENT OF VISUAL ($g/cm^2/min^{1/2}$)
Mortar (M1)	0.201	0.607
Mortar (M2)	0.318	1.103
Mortar (M3)	0.047	0.239
Tufa stone	0.309	0.921

the unique capillary imbibition characteristics of the repair mortar and the tufa stone, soluble salts might migrate and precipitate through their interfacial zone, potentially accelerating the deterioration of the older stone.

3.4.3. Gas and water permeability

The gas and water permeability co-efficient was shown in Figure 13 and Figure 14 for different mortars (M1, M2 & M3) and tufa stones. These statistics demonstrate that, in similarity to the produced mortar M3 and the prepared mortar M1, the prepared mortar M2 showed greater coefficients of gas and water permeability at every step. As can be seen in Figure 14, mortar M2's gas permeability coefficient was higher than that of the tufa stone. This confirms even more the previous claim about its composition making it appropriate for usage with old stone. Higher water and gas permeability in the repair mortar than in the old masonry causes less water to pass through the pores in the stone because water evaporates over the mortar's openings more quickly [39]. The significant and comparable total permeabilities of M2 and the tufa stone, as indicated in Table 4, suggest improved permeability, which encourages rapid drying and reduces the chance of cracks, which affects durability. While a larger amount of binder decreases porosity inside the binder matrix, the addition porosity is increased by aggregate and facilitates the passage of gas and water [13]. Increasing the amount of lime in mortar as opposed to cement allows for greater fluid permeability by forming a larger open-pore structure. Water flow is greatly impacted by this and is essential for repair mortars. Water, as everyone knows, is a major factor in masonry degradation in a variety of ways. As such, the mortar ought to demonstrate a comparable or even greater ability to transfer water than the tufa stone. This suggests that a mortar with a less water transmission capacity than a tufa stone will not discharge water as quickly as a tufa stone.

3.4.4. Microstructural analysis of mortar mix

Based on the above experimental studies, the mortar M1 is very good in compressive and flexural strength compared to other mortar mixes (M2 and M3). Also, the M2 mortar mix shows very low strength in all experimental studies. Hence, the microstructural analysis was conducted for M1 and M2 mortar mixes and the results are discussed below.

XRD analysis – Using the M1 and M2 mortar mixes including tufa stone powder, an X-ray diffraction examination was performed to investigate the corrosive products that were produced in the concrete as a result of sulfate attack. Figure 15 displays the diffractograms from XRD. In comparison to the M2 sample (Second picture), the first image shows lower intensity peaks of C-S-H and portlandite in the M1 sample, which was exposed to 200 cycles. Furthermore, minute levels of thenardite and gypsum were found in the first picture. The substance's intensity peaks increased upon exposure, signifying the cyclic sulfate exposure-induced creation of gypsum, thenardite, and the material. C-S-H and portlandite are consumed as a result of this procedure. The XRD findings suggest that the M1 mix crystalline structures are higher than the M2 mix. The M1 mix's peaks were in good agreement with the 80, 110, 60, 40, 30, and 20 hkl planes at 2θ, corresponding to 140, 210, 260, 291, 370, and 450, respectively. This attests to the peaks in the M1 mix having substantially greater intensities than those in the M2 mix.

SEM analysis – The SEM pictures of the M1 and M2 mortar mixes are shown in Figure 16, where the different ratios of silica sand and tufa stone powder are visible. The microstructural features of cement-based materials have a major impact on the hardened properties of concrete. The concrete microstructure and matrix morphology were revealed by the SEM analysis. After 28 days, two SEM micrographs were produced for the M1 and M2 mixes. The M1 mortar mix's microscopic picture is presented in the first figure, which shows a denser and more uniform microstructure than the M2 mix, which is depicted in the second figure. With the smaller grains in the M2 mix considerably lowering pore size, the hydration process aids in the pore structure's

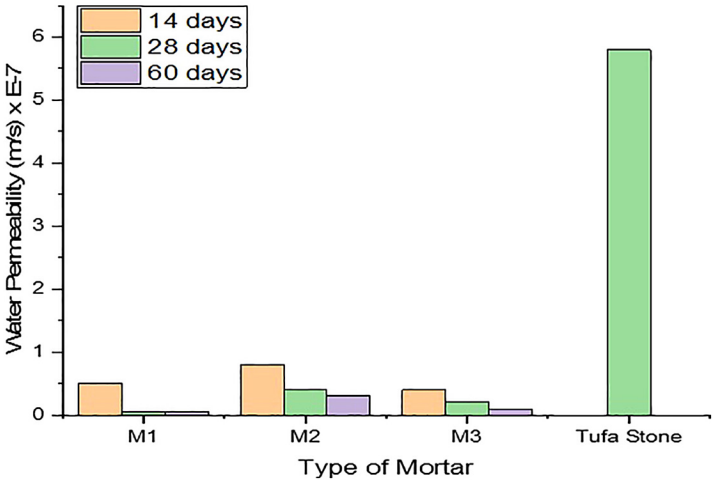

Figure 13: Tufa stone and mortar – water permeability at the ages of 14, 28 and 60 days.

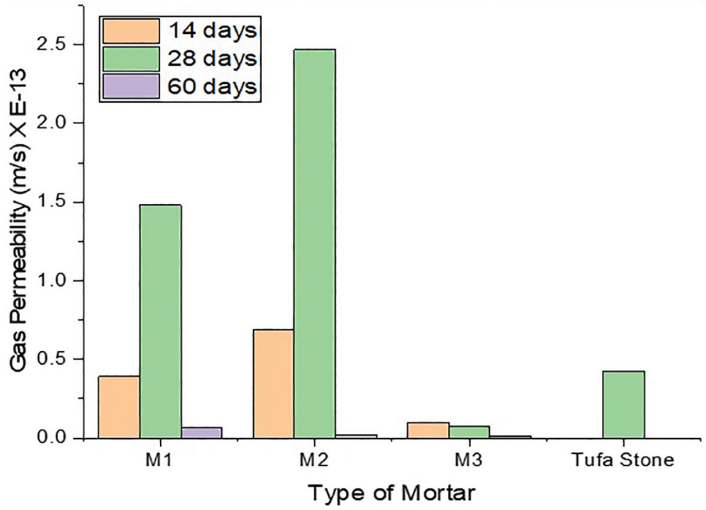

Figure 14: Tufa stone and mortar – gas permeability at the ages of 14, 28 and 60 days.

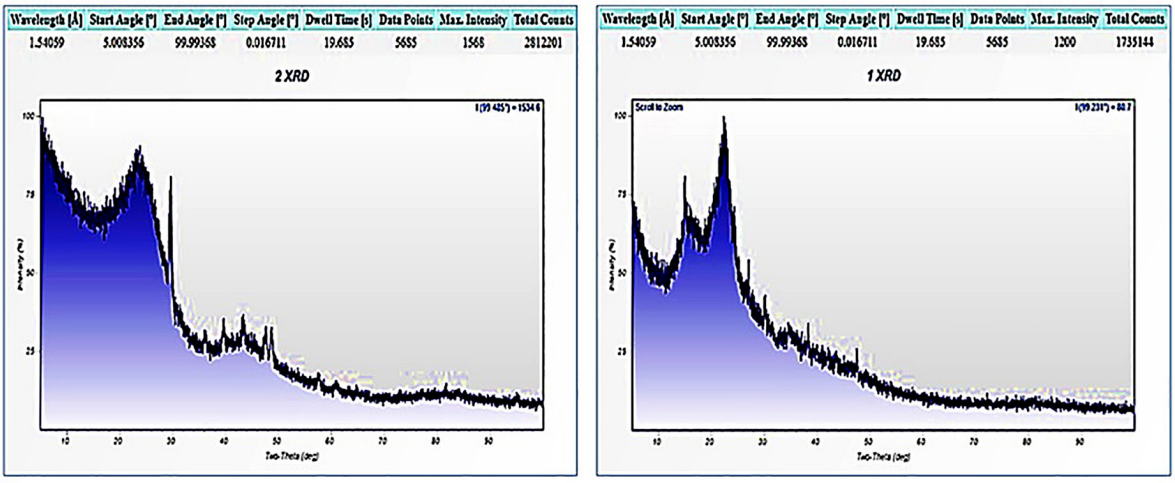

Figure 15: XRD spectra of M1 and M2 mortar mix with tufa stone powder.

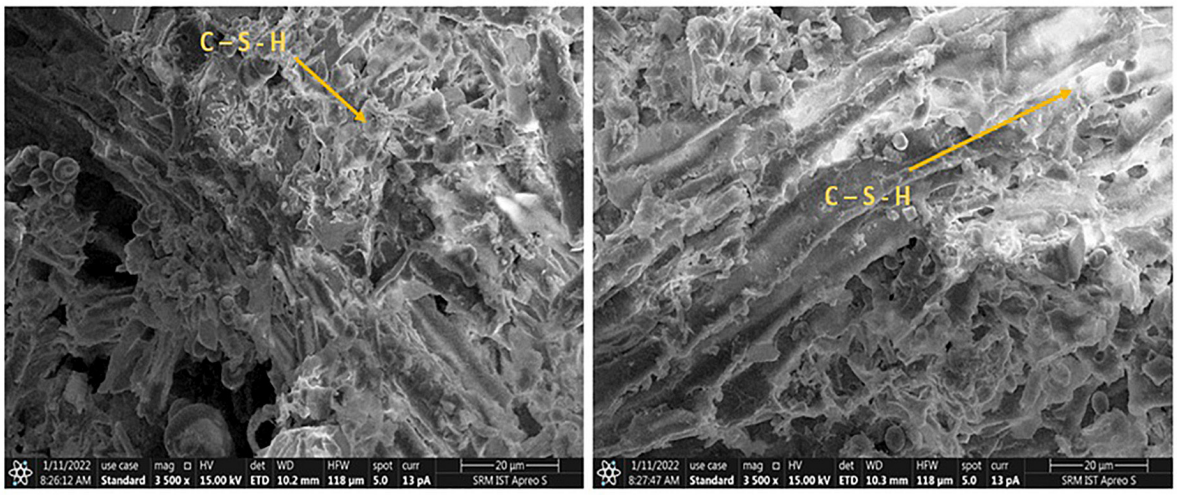

Figure 16: SEM images of M1 and M2 mortar mix with tufa stone powder.

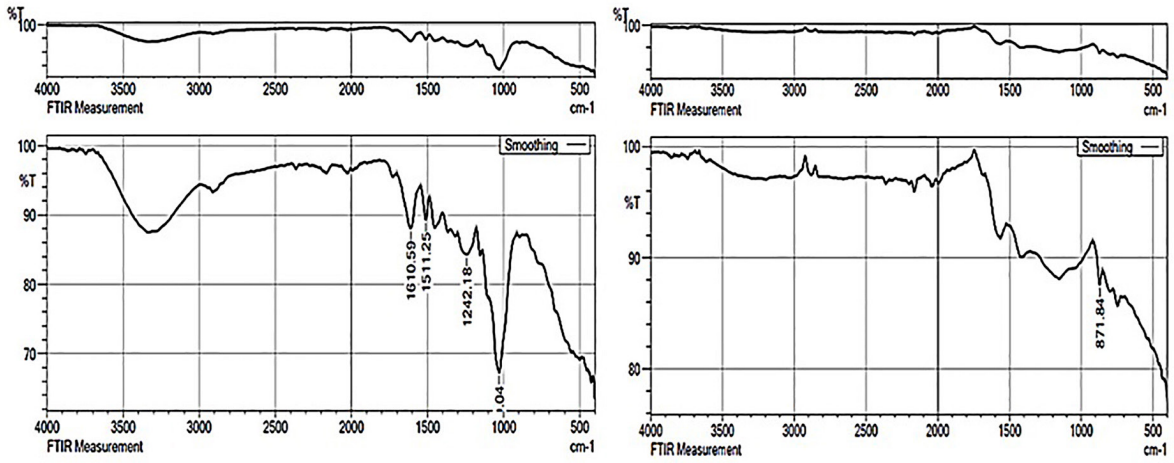

Figure 17: FTIR images of M1 and M2 mortar mix with tufa stone powder.

refining. According to experimental findings pertaining to mechanical qualities, the mixture that contained 50% of the M1 mix performed well in terms of compressive strength. Its increased strength is attributed to the C-S-H gel that is present in this combination.

FTIR studies – The FTIR spectra of the M1 and M2 mortar mixture and the powdered tufa stone is shown in Figure 17. The –OH group in this picture is responsible for the asymmetric absorption peak in the 3235–3730 cm^{-1} range. The peak at 3481 cm^{-1} in this area indicates the stretching vibration of the hydroxyl (–OH) and carboxyl (–COOH) groups in the M1 mortar mix. The methyl and methylene groups' distinctive peak levels of absorption were found at a number of peaks, including 2754, 1391, and 1317 cm^{-1}. Additionally, the stretching vibration of –C=O– at the peak of 1692 cm^{-1} indicated the existence of the ester group. Furthermore, the polyether –C–O–C– stretching vibration is responsible for the unique absorption peak in the M1 mix at 1107 cm^{-1}. The hydroxyl (–OH) stretching vibration is responsible for the asymmetric peak observed in the 3115–3655 cm^{-1} area of M2's FTIR spectra, which are displayed in the second section of the figure. The absorption peak at 3448 cm^{-1} shows evidence of carboxyl (–COOH) and hydroxyl (–OH) groups. The distinct methylene group absorption peaks may be seen at 2720, 1385, and 1257 centimeters. Because of the stretching of the –C=O-groups, the ester group is also located at 1729 cm^{-1}. Furthermore, the polyether –C–O–C– stretching vibration in M2 mortar mix is considered responsible for the unique absorption peak at 1107 cm^{-1}. More functional groups are present in the M1 mix than in the M2 mix, according to the experimental investigation.

4. CONCLUSION

The aim of this investigation was to determine whether tufa stone powder could be used to make mortar in lieu of some of the fine aggregate. Based on the deductions, mortar M2, which had a lower percentage of binder (15%) and a higher percentage of tufa powder substitution (42%), was found to be the most suitable and compatible option for historic monuments built of tufa stone.

The following succinctly outlines the reasoning for this conclusion:

- Mortar M2, the most porous of the mortars tested, with a single pore diameter peak that is somewhat smaller than the tufa stone. They have similar overall porosities in spite of this. This mortar has a high porosity, which allows salts to crystallize easily, especially when pressure is applied.
- Mortar M2 is a great preservation material due to its decreased compressive and flexural strengths. This feature reduces the possibility that cracks would emerge and permits the mortar to deteriorate without compromising the integrity of the old stone.
- The reduced shear strength where this mortar meets the tufa stone safeguards historic sites. It guarantees a good bond between the brickwork and the mortar, demonstrating the mortar's resistance to dynamic loads and shear stresses.
- At the mortar-stone interface, a lower adhesive strength is shown by mortar M2's decreased ultrasonic pulse velocity. This intrinsic bond between the different mortar constituents helps to slow down the aging process of the old stone.
- The thermal behavior of mortar M2 is similar to that of tufa stone, indicating that it is more effective in reducing stresses resulting from variations in the climate at the sites of contact.
- This mortar appears to have limited water movement based on the similar capillary absorption behavior seen in both the tufa stone and this mortar. As so, there will be less opportunity for soluble salts to seep through the mortar-stone interface.
- Over a range of cure times, mortar M2 showed permeability coefficients for gases and water that were quite similar to those of the tufa stone. The quick evaporation of these materials through this mortar's pores may greatly reduce the passage of gas and water through the tufa stone's pore structure.
- In addition, building on the results of this investigation, future research will examine how well the mortar that was developed works in conjunction with tufa stone, as well as how well it performs in salt tests and how durability evaluations might enhance the analysis.

5. BIBLIOGRAPHY

[1] MARAS, M.M., KOSE, M.M., RIZAOGLU, T., "Microstructural characterization and mechanical properties of Volcanic Tuff (Malatya, Turkey) used as building stone for the restoring cultural heritage", *Periodica Polytechnica. Civil Engineering*, v. 65, n. 1, pp. 309–319, 2020. doi: http://doi.org/10.3311/PPci.16977.

[2] AL-OMARI, A., KHATTAB, S., "Characterization of building materials used in the construction of historical Al-Omariya Mosque Minaret in Mosul's Old City, Iraq", *Journal of Building Engineering*, v. 33, pp. 101645, 2021. doi: http://doi.org/10.1016/j.jobe.2020.101645.

[3] BROUARD, Y., BELAYACHI, N., HOXHA, D., *et al*., "Mechanical and hygrothermal behavior of clay-sunflower (*Helianthus annuus*) and rape straw (*Brassica napus*) plaster bio- composites for building insulation", *Construction & Building Materials*, v. 161, pp. 196–207, 2018. doi: http://doi.org/10.1016/j.conbuildmat.2017.11.140.

[4] SANTOS, A.R.l., VEIGA, M.R.S., SILVA, A.M.S., *et al*., "Tensile bond strength of lime-based mortars: the role of the microstructure on their performance assessed by a new non-standard test method", *Journal of Building Engineering*, v. 29, pp. 101136, 2020. doi: http://doi.org/10.1016/j.jobe.2019.101136.

[5] MARAVELAKI-KALAITZAKI, P., BAKOLAS, A., KARATASIOS, I., *et al*., "Hydraulic Lime mortars for the restoration of historic masonry in Crete", *Cement and Concrete Research*, v. 35, n. 8, pp. 1577–1586, 2005. doi: http://doi.org/10.1016/j.cemconres.2004.09.001.

[6] BARATTA, A., CORBI, I., CORBI, O., "Bounds on the Elastic Brittle solution in bodies reinforced with FRP/FRCM composite provisions", *Composites. Part B, Engineering*, v. 68, pp. 230–236, 2015. doi: http://doi.org/10.1016/j.compositesb.2014.07.027.

[7] MASCIOTTA, M.-G., ROQUE, J.C.A., RAMOS, L.F., *et al*., "A multidisciplinary approach to assess the health state of heritage structures: the case study of the Church of Monastery of Jerónimos in Lisbon",

Construction & Building Materials, v. 116, pp. 169–187, 2016. doi: http://doi.org/10.1016/j.conbuildmat.2016.04.146.

[8] AMERICAN SOCIETY FOR TESTING AND MATERIALS, *ASTM D 2845-05 – standard test method for laboratory determination of pulse velocities and ultrasonic elastic constants of rock*, West Conshohocken, ASTM, 2005. doi: http://doi.org/10.1520/D2845-05.

[9] EUROPEAN COMMITTEE FOR STANDARDIZATION, *EN 459-1:2015 – building lime – part 1: definitions, specifications and conformity criteria*, Brussels, CEN, 2015.

[10] SINGH, Y., VYAS, A.K., SYED AHMED KABEER, K.I., "Compressive strength evaluation of mortars containing ISF Slag and marble powder", *Materials Today: Proceedings*, v. 4, n. 9, pp. 9635–9639, 2017. doi: http://doi.org/10.1016/j.matpr.2017.06.239.

[11] EUROPEAN COMMITTEE FOR STANDARDIZATION, *LST EN 1015-11 – methods of test for mortar for masonry – part 11: determination of flexural and compressive strength of hardened mortar*, Brussels, CEN, 2004.

[12] AFNOR Association, *NF P94-420 – roches-détermination de la résistance à la compression uniaxial* [rocks – determination of uniaxial compressive strength], Paris, AFNOR, 2000.

[13] Al-OMARI, A., ABDULKAREEM, O.M., ALDAOOD, A., *et al*., "Impact of tufa stone powder as a partial replacement of aggregate on the mechanical performance and durability of repair mortar", *Periodica Polytechnica. Civil Engineering*, v. 66, n. 2, pp. 433–444, 2022. doi: http://doi.org/10.3311/PPci.19146.

[14] AMERICAN SOCIETY FOR TESTING AND MATERIALS, *ASTM D3080-11 – standard test method for direct shear test of soils under consolidated drained conditions*, West Conshohocken, ASTM, 2011.

[15] AMERICAN SOCIETY FOR TESTING AND MATERIALS, *ASTM D5930-97 – standard test method for thermal conductivity of plastics by means of a transient line-source technique*, West Conshohocken, ASTM, 2001.

[16] AFNOR Association, *NF-P94-411 – roches-détermination de la vitesse de propagation des ondes ultrasonores en laboratoire – méthode par transparence* [rocks – determination of the speed of propagation of ultrasonic waves in the laboratory – transparency method]), Paris, AFNOR, 2002.

[17] EUROPEAN COMMITTEE FOR STANDARDIZATION, *EN 1925:1999 – natural stone test methods – determination of water absorption coefficient by capillarity*, Brussels, CEN, 1999.

[18] KIM, J., "Construction and demolition waste management in Korea: recycled aggregate and its application", *Clean Technologies and Environmental Policy*, v. 23, n. 8, pp. 2223–2234, 2021. doi: http://doi.org/10.1007/s10098-021-02177-x.

[19] DUAN, Z.H., POON, C.S., "Properties of recycled aggregate concrete made with recycled aggregates with different amounts of old adhered mortars", *Materials & Design*, v. 58, pp. 19–29, 2014. doi: http://doi.org/10.1016/j.matdes.2014.01.044.

[20] KIM, Y., HANIF, A., KAZMI, S.M.S., *et al*., "Properties enhancement of recycled aggregate concrete through pretreatment of coarse aggregates – Comparative assessment of assorted techniques", *Journal of Cleaner Production*, v. 191, pp. 339–349, 2018. doi: http://doi.org/10.1016/j.jclepro.2018.04.192.

[21] JANG, H., KIM, J., SICAKOVA, A., "Effect of aggregate size on recycled aggregate concrete under equivalent mortar volume mix design", *Applied Sciences*, v. 11, n. 23, pp. 11274, 2021. doi: http://doi.org/10.3390/app112311274.

[22] SEO, D.S., CHOI, H.B., "Effects of the old cement mortar attached to the recycled aggregate surface on the bond characteristics between aggregate and cement mortar", *Construction & Building Materials*, v. 59, pp. 72–77, 2014. doi: http://doi.org/10.1016/j.conbuildmat.2014.02.047.

[23] HOEPFNER, J.C., PORTO, R.C.T., ZIGOSKI UCHÔA, P., *et al*., "Dynamical mechanical properties of polyvinylbutyral nanocomposites: a comparison between different nano-carbon reinforcements", *Matéria*, v. 27, n. 2, e13223, 2022. doi: http://doi.org/10.1590/s1517-707620220002.1323.

[24] DE JUAN, M.S., GUTIÉRREZ, P.A., "Study on the influence of attached mortar content on the properties of recycled concrete aggregate", *Construction & Building Materials*, v. 23, n. 2, pp. 872–877, 2009. doi: http://doi.org/10.1016/j.conbuildmat.2008.04.012.

[25] AKYÜNCÜ, V., AVŞAR, Y.E., "Physical and mechanical properties of alkali activated mortars produced using different types of fly ash", *European Journal of Engineering and Applied Sciences*, v. 5, n. 1, pp. 16–21, 2022. doi: http://doi.org/10.55581/ejeas.1125144.

[26] SILVA, T.F., NASCIMENTO, M.A., MOURA, E.F.C., *et al*., "Influence of the cooling process on the physicochemical properties of ladle furnace slag, used in the replacement of Portland cement", *Matéria*, v. 27, n. 3, e20220089, 2022. doi: http://doi.org/10.1590/1517-7076-rmat-2022-0089.

[27] AFSHINNIA, K., POURSAEE, A., "The potential of ground clay brick to mitigate Alkali-Silica Reaction in mortar prepared with highly reactive aggregate", *Construction & Building Materials*, v. 95, pp. 164–170, 2015. doi: http://doi.org/10.1016/j.conbuildmat.2015.07.155.

[28] ARORA, S., SINGH, S.P., "Flexural fatigue performance of concrete made with recycled concrete aggregates and ternary blended cements", *Journal of Sustainable Cement Based Materials*, v. 7, n. 3, pp. 182–202, 2018. doi: http://doi.org/10.1080/21650373.2018.1471423.

[29] AHO, I.M., NDUBUBA, E.E., "Compressive and flexural strength of cement mortar stabilized with raffia palm fruit peel (RPEP)", *Global Journal of Engineering Research*, v. 14, n. 1, pp. 1–7, 2015. doi: http://doi.org/10.4314/gjer.v14i1.1.

[30] YEON, K.S., KIM, K.K., YEON, J., *et al*., "Compressive and flexural strengths of EVA-modified mortars for 3D additive construction", *Materials*, v. 12, n. 16, pp. 2600, 2019. doi: http://doi.org/10.3390/ma12162600.

[31] ŁĄTKA, D., "Prediction of mortar compressive strength based on modern minor-destructive tests", *Materials*, v. 16, n. 6, pp. 2402, 2023. doi: http://doi.org/10.3390/ma16062402. PubMed PMID: 36984282.

[32] KATZER, J., SZATKIEWICZ, T., "Effect of 3D printed spatial reinforcement on flexural characteristics of conventional mortar", *Materials*, v. 13, n. 14, pp. 3133, 2020. doi: http://doi.org/10.3390/ma13143133. PubMed PMID: 32674343.

[33] KIZILKANAT, A.B., KABAY, N., AKYÜNCÜ, V., *et al*., "Mechanical properties and fracture behavior of basalt and glass fiber reinforced concrete: an experimental study", *Construction & Building Materials*, v. 100, pp. 218–224, 2015. doi: http://doi.org/10.1016/j.conbuildmat.2015.10.006.

[34] ISEBAERT, A., VAN PARYS, L., CNUDDE, V., "Composition and compatibility requirements of mineral repair mortars for stone: a review", *Construction & Building Materials*, v. 59, pp. 39–50, 2014. doi: http://doi.org/10.1016/j.conbuildmat.2014.02.020.

[35] PÁPAY, Z., TÖRÖK, Á., "Effect of thermal and freeze-thaw stress on the mechanical properties of porous limestone", *Periodica Polytechnica. Civil Engineering*, v. 62, n. 2, pp. 423–428, 2017. doi: http://doi.org/10.3311/PPci.11100.

[36] GERMINARIO, L., TÖRÖK, Á., "Surface weathering of tuffs: compositional and microstructural changes in the building stones of the medieval castles of Hungary", *Minerals*, v. 10, n. 4, pp. 376, 2020. doi: http://doi.org/10.3390/min10040376.

[37] THOMAS, C., LOMBILLO, I., SETIEN, J., *et al*., "Characterization of materials with repellents and consolidates from a historic building", *Journal of Materials in Civil Engineering*, v. 25, n. 11, pp. 1742–1751, 2013. doi: http://doi.org/10.1061/(ASCE)MT.1943-5533.0000747.

[38] BÖKE, H., ÇIZER, O., IPEKOĞLU, B., *et al*., "Characteristics of lime produced from limestone containing diatoms", *Construction & Building Materials*, v. 22, n. 5, pp. 866–874, 2008. doi: http://doi.org/10.1016/j.conbuildmat.2006.12.010.

[39] ZENG, Q., LI, K., FEN-CHONG, T., *et al*., "Effect of porosity on thermal expansion coefficient of cement pastes and mortars", *Construction & Building Materials*, v. 28, n. 1, pp. 468–475, 2012. doi: http://doi.org/10.1016/j.conbuildmat.2011.09.010.